



HAL
open science

Thermal Analytical Modelling of the Heat Transfer Through a Power PCB Dedicated to a High Current Density Modular Converter

Gaël Pongnot, Mickael Petit, Marie-Christine Duluc, Fabien Adam, Clement Mayet, Denis Labrousse

► To cite this version:

Gaël Pongnot, Mickael Petit, Marie-Christine Duluc, Fabien Adam, Clement Mayet, et al.. Thermal Analytical Modelling of the Heat Transfer Through a Power PCB Dedicated to a High Current Density Modular Converter. PCIM Europe 2022, International Exhibition and Conference for Power Electronics, Intelligent Motion, Renewable Energy and Energy Management, May 2022, Nuremberg, Germany. 10.30420/565822124 . hal-03764888

HAL Id: hal-03764888

<https://hal.science/hal-03764888>

Submitted on 30 Aug 2022

HAL is a multi-disciplinary open access archive for the deposit and dissemination of scientific research documents, whether they are published or not. The documents may come from teaching and research institutions in France or abroad, or from public or private research centers.

L'archive ouverte pluridisciplinaire **HAL**, est destinée au dépôt et à la diffusion de documents scientifiques de niveau recherche, publiés ou non, émanant des établissements d'enseignement et de recherche français ou étrangers, des laboratoires publics ou privés.

Thermal Analytical Modelling of the Heat Transfer Through a Power PCB Dedicated to a High Current Density Modular Converter

Gaël Pongnot¹, Mickaël Petit^{1,2}, Marie-Christine Duluc³, Fabien Adam¹, Clément Mayet^{1,2}, Denis Labrousse^{1,2}

¹ Université Paris-Saclay, ENS Paris-Saclay, CNRS, SATIE, 91190, Gif-sur-Yvette, France

² SATIE, UMR 8029, Cnam, F 75003, Paris, France, HESAM Université

³ Lafset, Cnam, F 75003, Paris, France, HESAM Université

Corresponding author: Gaël Pongnot, gael.pongnot@ens-paris-saclay.fr

Abstract

This work is based on an innovative converter structure for an automotive application. A major constraint is the cooling. A nondimensionalization and an analytical resolution of a thermal problem applied to power electronics are proposed. A study of the influence of the geometrical parameters on thermal resistance is carried out to understand the underlying phenomena. Two sizing methods are proposed, based on charts calculated from the proposed resolution. An example of an application based on the initial problem is presented and compared to a finite element simulation.

1 Introduction

Nowadays, Zero-Emission Vehicles (ZEV) such as Battery Electric Vehicles (BEV) are critical players in facing current challenges in energy-saving and greenhouse gas emission. Further improvements in terms of efficiency, rechargeability, reliability, reconfigurability, compacity, and second life possibility (especially for the battery) are crucial to improve the performances, reduce the carbon footprint, and increase the market penetration of BEV [1]–[3].

The traction system of conventional BEV combines a high-voltage battery pack (typically 400 V) with a Voltage Source Inverter (VSI) and an Electric Machine (EM). Additionally, an external charger is required to charge the battery. Previous papers have proposed another architecture using Multi-Level Inverter with Integrated Battery (MLI-IB) for automotive applications [4], [5]. The significant advantages of this architecture are quasi-sinusoidal output voltages, an active balancing of cells while operating, and an increase in safety. The challenge is to develop a low-cost and compact H-Bridge. This reason leads to the use of a PCB substrate.

Switches are mounted on the top side of the PCB, a cold plate located on the bottom side ensures

cooling. The transistors must be maintained at an acceptable junction temperature (100 to 120 °C) despite a 150 A_{RMS} current in thermal steady state. Due to the high heat flux to be dissipated and the technological choice of the PCB substrate, the cooling of these components is the dimensional constraint of this power converter.

Traditionally, steady-state thermal cooling is studied using simple empirical models (diffusion cone) or finite element simulations. Analytical resolutions are often avoided [6]. Empirical models are not based on a rigorous formulation of a heat conduction problem, which leads to large error margins [7]–[9]. As for numerical simulations, they allow detailed modeling of complex systems. However, it is difficult to carry out a preliminary study or an optimization, for which many electrical and thermal parameters remain undetermined. Moreover, simulation times are sometimes prohibitive.

This paper proposes addressing the geometrical sizing of a heat sink associated with any chip. A two-dimensional approach and steady-state condition are considered. An analytical solution is developed considering heat conduction for a thermally and electrically isotropic rectangular heatsink. A nondimensionalization reduces the number of physical parameters and simplifies the analysis.

The influence of dimensionless parameters on the thermal resistance of the heatsink and on the heat flux spreading is studied to develop a decision aid. In particular, two methods are presented: the first allows the optimal dimensions of the heatsink to be obtained knowing the power component and its operating point; the second one gives the operating limit point of the component knowing the available cooling source.

2 Intelligent battery inverter system (IBIS)

The IBIS structure combines power converters and battery cells to create a Multi-Level Inverter with Integrated-Battery. It aims to fulfill the roles of VSI, BMS, active cells balancing, charger, and ensures that each cell is managed individually.

2.1 Multi-Level Inverter with Integrated-Battery (MLI-IB)

The MLI-IB integrates battery cells into cascaded H-Bridge Converters (HBC) and supplies the EM of the traction system. Figure 1 shows the cascading of these modules, consisting of a battery cell and an HBC, to form one phase of a MLI-IB capable of powering an EM. The modularity of the MLI-IB offers opportunities for significant reconfigurations and the recovery and reuse of used battery cells, which is a sustainable way of using them considering the current global challenges of energy storage.

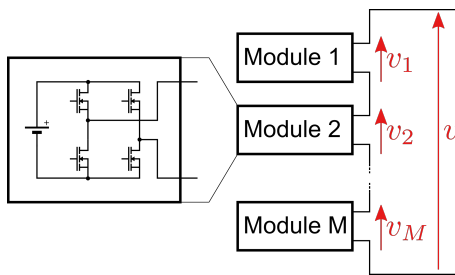


Fig. 1: Structure of a MLI-IB

In addition, different controls can be proposed, especially without using the PWM technique, which can potentially reduce the overall losses of the power electronics devices. Figure 2 shows one of these possible controls, the output waveform of the MLI-IB is very close to the reference sinusoid, which reduces the need for filtering compared to a 2-or-3-levels PWM control. The output voltage of the modules takes the values $+V_{\text{cell}}$, $-V_{\text{cell}}$ or 0

as expected. This figure also shows that the lower the module index is, the higher its provided power is. This disequilibrium need to be considered in the final command [5]. Despite the complexity of this topology, the MLI-IB can, therefore, potentially offer significant improvements compared to the conventional topology.

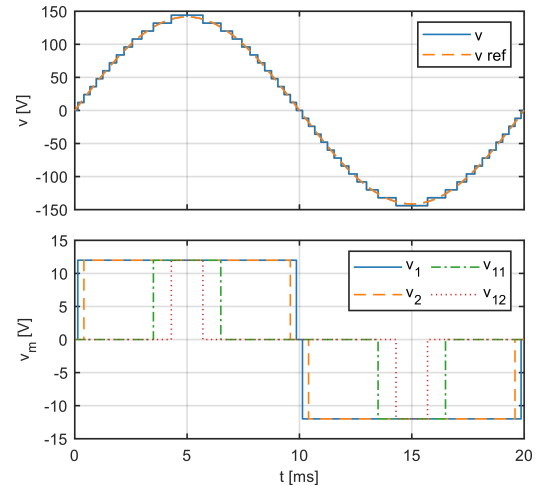


Fig. 2: Principle of a MLI-IB

2.2 H-bridge on PCB substrate

The HBC is constituted of four MOSFET switches that allow a three-level output voltage: $+V_{\text{cell}}$, $-V_{\text{cell}}$ or 0V. Whatever the output voltage, the phase current flows through two switches of the module. The maximum current flowing is equal to $150 A_{\text{RMS}}$.

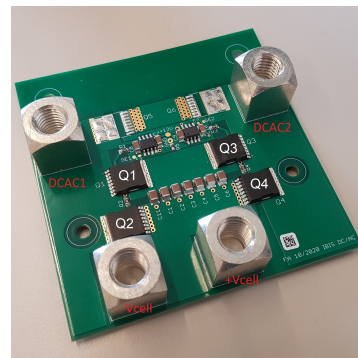


Fig. 3: H-bridge on PCB substrate

The first design of a 4-layer PCB is realized using IPC-2221 standards, in particular for thermal limitations (Fig. 3). The MOSFET switches are provided by ON-semi (FDBL9401-F085, 40V, 300A, $0.65 m\Omega$) manufactured in TOLL package (MO-299A). Switches are mounted on the top side of the PCB, a cold plate located on the bottom side ensures cooling. The heat transfer from the MOS-

FETs to the heatsink is ensured by copper-plated through holes (Fig. 4).

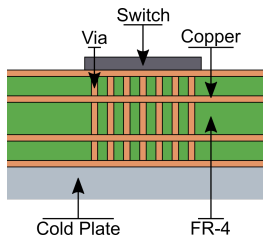


Fig. 4: Cross-section of a 4-layer pcb

3 Thermal modelling

Cooling is, as mentioned above, the constraint that sets the operating limit of the HBC. However, this phenomenon is generally poorly understood. IPC standards give guidelines, empirical models such as the diffusion cone provide attempts at physical explanation, finite element methods can lead to quite accurate results, but in any case, the influence of the parameters is difficult to grasp.

3.1 Finite element method

Once a circuit prototype has been built in a CAD program such as Altium, a 3D model can be extracted for use in a finite element simulation program. These simulations allow to couple electrokinetic and heat transfer aspects to calculate losses in transistors and tracks. It is, for example, the case of the simulation presented in Fig. 5.

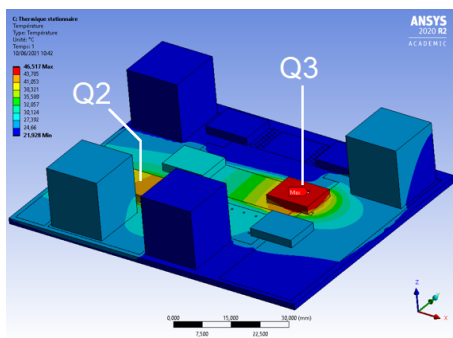


Fig. 5: ANSYS Electro-thermal simulation exemple (red: 46 °C, blue: 20 °C)

The configuration where Q2 and Q3 let flow the current to provide the tension $+V_{cell}$ is simulated. These simulations show two hot spots corresponding to Q2 and Q3. However, the transistor Q3 (46 °C) presents a higher temperature than Q2 (40 °C) without any apparent reason. Therefore, the

board will have to be redesigned to eliminate this imbalance. This improvement process is sub-optimal because it requires human intervention at each iteration (to design the map) and time-consuming finite element simulations. Moreover, the modifications can be misdirected or counterproductive if the phenomena involved in this imbalance are not understood. That is why this article proposes a more theoretical approach to understand better the issues and the phenomenon involved.

3.2 Mathematical modelling

The studied system is a plate of thermal conductivity k , thickness t , infinite length and width $2W$. On this plate a homogeneous heat flux q_0'' is imposed on a central part, of width $2w$, of the lower face. A heat transfer coefficient h is imposed on the upper face. Figure 6 illustrates this system.

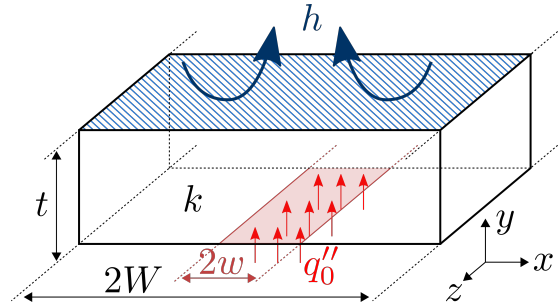


Fig. 6: 3D physical model

The problem is representative and straightforward of classical power electronics devices: a component dissipates a specific power on the surface of a substrate, such as a DBC (Direct Bonded Copper), PCB (Printed Circuit Board), or MCPCB (Metal Core Printed Circuit Board), which is cooled on the opposite side by a finned heat sink or a fluid cold plate.

The material is considered as homogeneous, with an isotropic thermal conductivity and independent of temperature. The heat transfer coefficient h and the heat flux q_0'' are assumed to be homogeneous on their application surfaces. The external environment is assumed to be at temperature T_∞ . The material properties are constant, so only the temperature increase $\Delta T = T - T_\infty$ is considered.

The power to be dissipated having for origin Joule losses in the component. It is interesting to introduce the equivalent resistance R and the RMS current I in the formulation of the problem. The

component, considered of square shape, has a surface area of $4w^2$. Equation (1) describes the link between the heat flux and the RMS current.

$$q_0'' = \frac{RI^2}{4w^2} \quad (1)$$

Some of the assumptions made are strong and questionable for the intended application, but the study is greatly simplified. Indeed, the symmetries and invariances allow reducing the problem to a 2D plane study, which the Fourier series can quickly solve. The results obtained will establish trends, which will be used for more complex geometries.

3.3 Resolution

The problem statement shows ten independent physical quantities: two geometric variables (x, y), one output quantity (ΔT) and seven parameters (W, w, t, k, I, R, h). The Vashy-Buckingham theorem then ensures that the problem can be reduced to an equivalent problem involving six dimensionless variables.

3.3.1 Nondimensionalization

The dimensionless variables are determined to simplify the expression of the boundary conditions. The quantities w, k, ρ , and R are considered fixed by our application. That is why they will be used as fundamental quantities. The new set of parameters is presented below. The problem is thus represented in Figure 7.

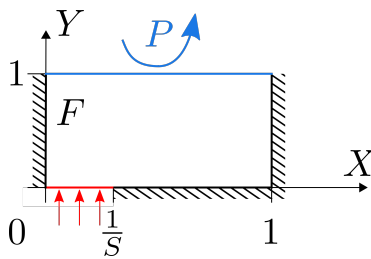


Fig. 7: 2D scaled physical model

The parameters of Equation (2) represent the dimensionless physical quantities associated with the problem: position and temperature. The parameters of Equation (3) are the dimensionless parameters determining the nature of the problem: F is a form factor, S is a spreading factor ($S \geq 1$), and P is a performance factor derived from Biot's number representing the ratio between conduction and convection resistance.

$$X = \frac{x}{W} \quad Y = \frac{y}{t} \quad \theta = \frac{4kw^2}{tRI^2} \Delta T \quad (2)$$

$$F = \frac{t}{w} \quad S = \frac{W}{w} \quad P = \frac{hw}{k} \quad (3)$$

Tables 1 and 2 summarize the ranges of admissible values of the different parameters of the problem. The deduction of the ranges of variation of the dimensionless parameters is necessary to restrict the study to only valuable ranges.

Tab. 1: Typical values of the physical quantities

Symbol	Min.	Typ.	Max.	Unit
W	w	50	200	mm
w	1	10	20	mm
t	10	100	30 000	μm
k	0.3	400	400	$\text{W m}^{-1} \text{K}^{-1}$
h	10	1000	6000	$\text{W m}^{-2} \text{K}^{-1}$
R	0.1	0.55	10	$\text{m}\Omega$
I		150		A

Tab. 2: Typical values of the dimensionless quantities

Symbol	Min.	Typ.	Max.
S	1	5	200
F	5×10^{-4}	0.01	30
P	25×10^{-6}	0.025	20

3.3.2 Resolution by Fourier series

The solution of the problem consists in finding the function $\theta(X, Y)$ which respects Equation (4) as well as the boundary conditions (Eq. (5)). The dimensionless temperature $\theta(X, Y)$ is searched in the form of a cosine Fourier series to match the symmetries of the problem.

$$\frac{F^2}{S^2} \frac{\partial^2 \theta}{\partial X^2} + \frac{\partial^2 \theta}{\partial Y^2} = 0 \quad (4)$$

$$\begin{aligned} \text{for } X = 0, \quad & \frac{\partial \theta}{\partial X} = 0 \\ \text{for } X = 1, \quad & \frac{\partial \theta}{\partial X} = 0 \\ \text{for } Y = 0, \quad & \frac{\partial \theta}{\partial Y} = \begin{cases} -1 & \text{if } X \in [0, \frac{1}{S}] \\ 0 & \text{else} \end{cases} \\ \text{for } Y = 1, \quad & \frac{\partial \theta}{\partial Y} + PF\theta = 0 \end{aligned} \quad (5)$$

$$\theta(X, Y) = \frac{1}{S} \left(1 - Y + \frac{1}{PF} \right) + \frac{Q}{F} \left(\frac{1}{PF} + \frac{1 - Y^2}{2} \right) + \sum_{n=1}^{+\infty} 2 \operatorname{sinc} \left(\frac{n\pi}{S} \right) \frac{\left(\frac{1}{S} - \frac{P}{n\pi} \right) e^{-\frac{Fn\pi}{S}(2-Y)} + \left(\frac{1}{S} + \frac{P}{n\pi} \right) e^{-\frac{Fn\pi}{S}Y}}{F \left(P + \frac{n\pi}{S} \tanh \frac{Fn\pi}{S} \right) \left(1 + e^{-2\frac{Fn\pi}{S}} \right)} \cos(n\pi X) \quad (6)$$

The result obtained is presented by Equation (6) in a form compatible with numerical calculations. It allows a direct calculation at any geometry point by truncating the Fourier series to the desired order.

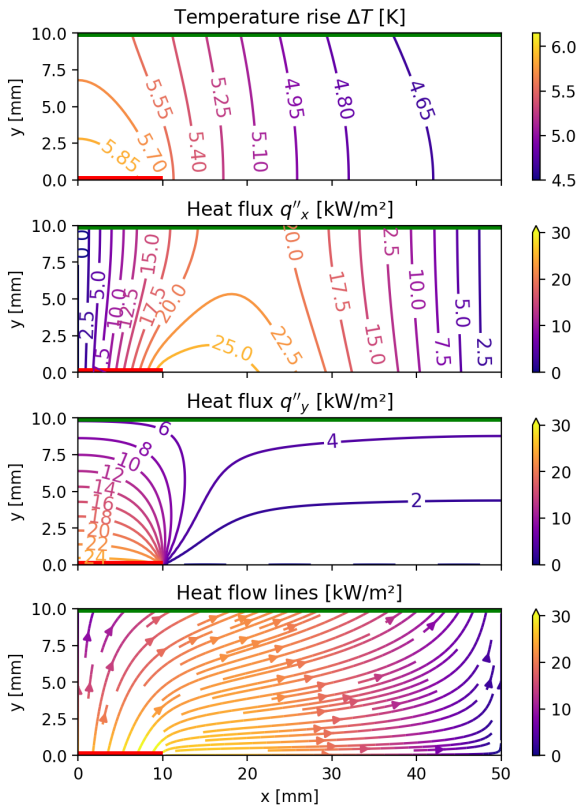
The numerical calculation is fast and reliable. As an illustration, the temperature and heat flux fields are plotted on Figure 8 in a particular configuration. The influence of the parameters is then easy to study in order to understand the physical consequences.

reference corresponds to the origin point, where the superheat is maximum $\theta_{\max} = \theta(0, 0)$. In the rest of the study, the quantity of interest will be $4kwR_{th} = F\theta(0, 0)$ because it is dimensionless.

$$R_{th} = \frac{\Delta T(0, 0)}{RI^2} = \frac{\Delta T(0, 0)}{4w^2q_0''} = \frac{1}{4kw} F\theta(0, 0) \quad (7)$$

4 Results and discussion

This section aims to extract relevant analyses for the targeted application from the previous analytical resolution. In particular, it will discuss the distribution of the heat flux in the conductor, the geometrical optimization of the thermal resistance, and the relevance of the solution towards real devices.



$$W = 50 \text{ mm}, w = 10 \text{ mm}, t = 10 \text{ mm}, h = 1000 \text{ W m}^{-2} \text{ K}^{-1}, \\ R = 1 \text{ m}\Omega, I = 100 \text{ A}, k = 400 \text{ W m}^{-1} \text{ K}^{-1}$$

Fig. 8: Temperature rise and heat flux fields

3.3.3 Thermal resistance

The quantity of interest for the power electronics engineer is the thermal resistance, the ratio between the temperature rise of the component and the power dissipated. This quantity is defined by Equation (7), the temperature rise chosen as

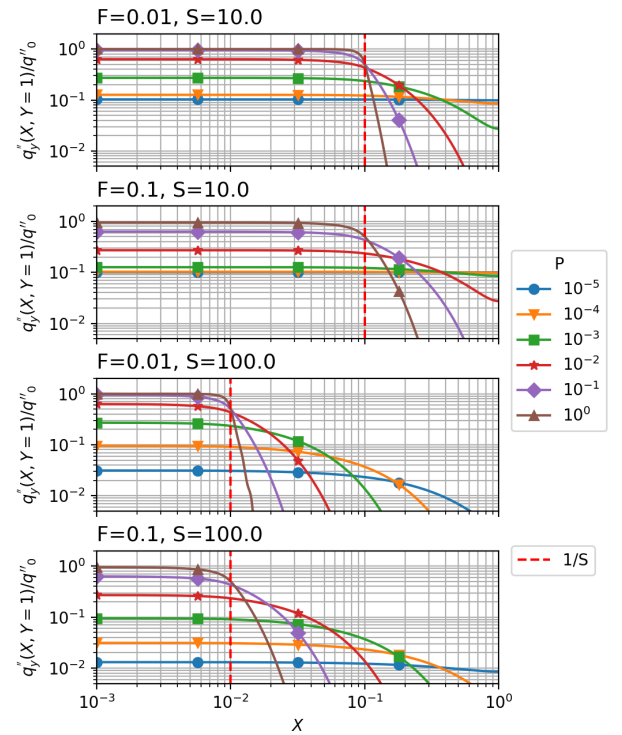


Fig. 9: Distribution of the vertical component of the heat flux on the upper wall

4.1 Flux spreading

Figure 9 allows apprehending the heat flux spreading, considering the distribution of the vertical component of the heat flux q''_y on the upper wall. The dotted vertical line represents the limit of the component. The commonly accepted result is found: when the heat transfer coefficient is low (performance factor $P \rightarrow 0$), the vertical component of the heat flux is homogenized, while when $P \rightarrow \infty$ it is concentrated at the vertical of the source. Similarly, the greater the thickness t , represented by the dimensionless factor form F , the better the spreading effect.

4.2 Parameters influence on thermal resistance

The thermal resistance R_{th} being the quantity of interest, the study of the influence of the parameters on this quantity is essential. Figures 10 and 11 present the dimensionless thermal resistance $4kwR_{th}$ as a function of the spread factor S . Figure 10 takes as parameters the form factor F , while Figure 11 focuses on the performance factor P .

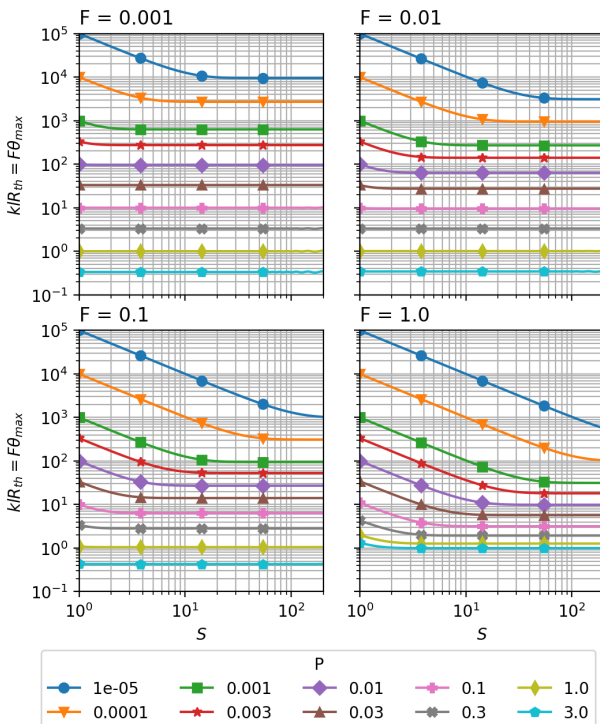


Fig. 10: Influence of P on $4kwR_{th}$

Two types of asymptotes are visible in Figure 10. The first type is the $1/S$ asymptotes which appear for small S , small P , and large F . This phe-

nomenon can be called the *spreader* effect: increasing the width W allows a better spreading of the heat flux on the upper wall and the use of a larger exchange surface with the cooling fluid. The second category is independent of S . It appears in the opposite cases to the previous one and reflects an effect of *thin layer*: the heat flux does not spread when increasing the width of the conductor because the transmission is favored in the vertical direction by a thin thickness and a high P .

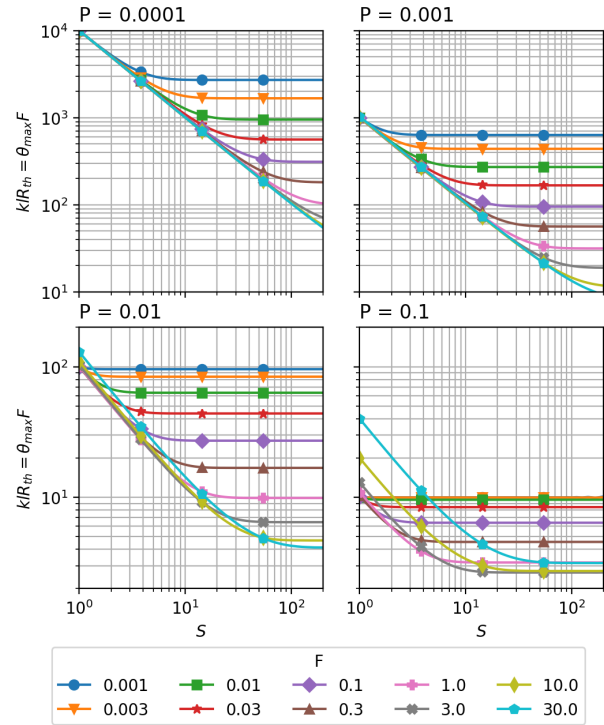


Fig. 11: Influence of F over $4kwR_{th}$

Figure 11 shows two types of asymptotes of the same order as before, but also sometimes a crossing of the curves for sufficiently large values of the performance factor P . In this case, for the same pair (S, P) , at least two configurations F can lead to the same thermal resistance value. This indicates that optimizations are possible. In particular, for $P = 0.1$, at $S = 5$ the values $F = 30$ and $F = 0.03$ lead to the same value $4kwR_{th} = 9$. Another criterion, such as volume minimization or heat capacity maximization (for the transient regime not studied here), is needed to select the most suitable configuration.

4.3 Abacus and dimensioning aid

Therefore, representing $4kwR_{th}$ in the (S, F) plane appears useful in order to obtain a network of level

lines (Fig. 12). Three evolution zones are highlighted: independent of S , independent of F , and independent of F/S . These curves show global minima, which can be used for optimization.

Finally, the empirical vision of the large and thick *spreader*, whose interest is clear when the cooling is not excellent, is confirmed. This figure shows, however, that there is no point in excessively widening the *spreader* as this will have no beneficial effect. Moreover, the excessive thickness increase can decrease performance when the cooling system is efficient (high value of P).

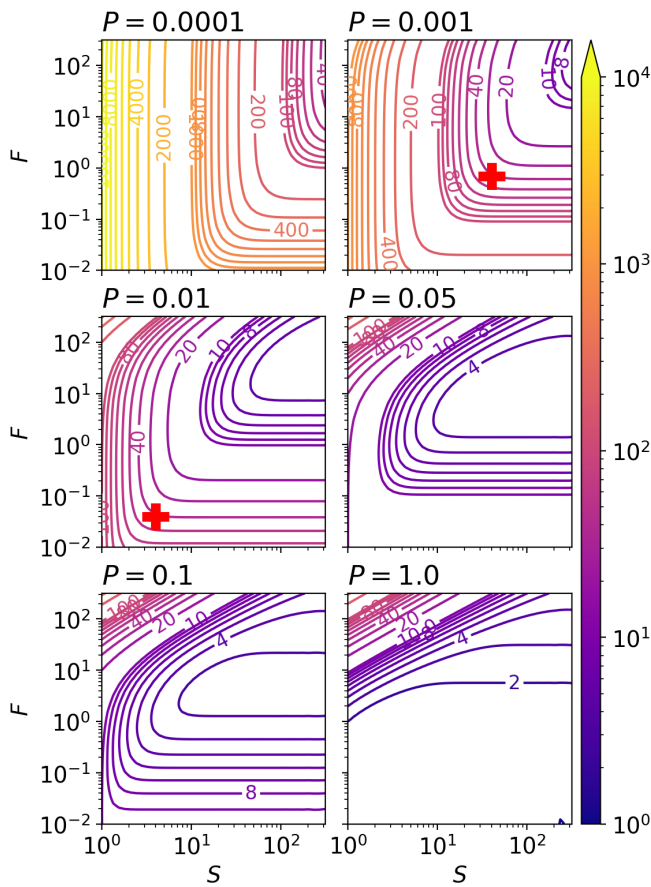


Fig. 12: Mapping of $4kwR_{th}(S, F)$ several values of P

These curves are used to develop sizing strategies for a cooling system designer. The maximum allowable current in the component is based on the search for width W , thickness t , and current I knowing the other parameters. The study begins by calculating P from the problem data, which allows the selection of the graph to be read in order to determine the pair (S, F) that minimizes the thermal resistance $4kwR_{th}$. The conversion into dimensional quantities concludes this method.

A second approach consists in determining the opti-

mal cooling (W , t , and h) and starts with the calculation of $4kwR_{th}$. The reading of the graphs allows to choose the triplet (S, F, P) according to the user's criteria and to deduce the dimensioned quantities.

4.4 Application

In order to illustrate the use of the previous methods, a cooling device at electric potential, made of a copper plate placed between the component and the heat exchanger, is studied. The specifications are inspired by the real problem presented in section 2 : $2w = 13$ mm, $k = 400$ K m⁻¹ W⁻¹ (copper), $\Delta T = 50$ K, $R = 0.55$ m Ω and $I = 150$ A. Then come $R_{th} = 4$ K W⁻¹, and $4kwR_{th} = 42 \simeq 40$. Optimization of the volume will first minimize the thickness t (F) and then the width W (S).

The search for the value $4kwR_{th} = 40$ in the charts leads to the cases $P = 1 \times 10^{-2}$ and $P = 1 \times 10^{-3}$. The point (S, F) is then determined by graphical reading, represented in Fig. 12. Then come the presented dimensionless triplet Equations (8) and (9), and consequently their dimensionless version Equations (10) and (11). The first triplet is characteristic of air-forced cooling, while the second one corresponds to air-free cooling. In order to minimize the size of the system and because of forced cooling is feasible, the first solution is chosen.

$$S = 4 \quad F = 4 \times 10^{-2} \quad P = 1 \times 10^{-2} \quad (8)$$

$$S = 40 \quad F = 7 \times 10^{-1} \quad P = 1 \times 10^{-3} \quad (9)$$

$$2W = 52 \text{ mm} \quad t = 0.26 \text{ mm} \quad h = 616 \text{ SI} \quad (10)$$

$$2W = 520 \text{ mm} \quad t = 9 \text{ mm} \quad h = 62 \text{ SI} \quad (11)$$

Figure 13 represents the temperature and heat flux distributions in the conductor for the conditions determined above. The maximum temperature rise is 49.1 °C, it is a few less than expected because the dimensionless thermal resistance was considered to be 40 and not 42. The temperature gradient is, in this case, purely horizontal, as shown by the relative magnitude difference of q''_x and q''_y . This temperature gradient is maximum at the edge of the chip, so at this place, the mechanical stresses will be the most important.

Of course, these results seem far for the intended application, but this is due to the assumptions made

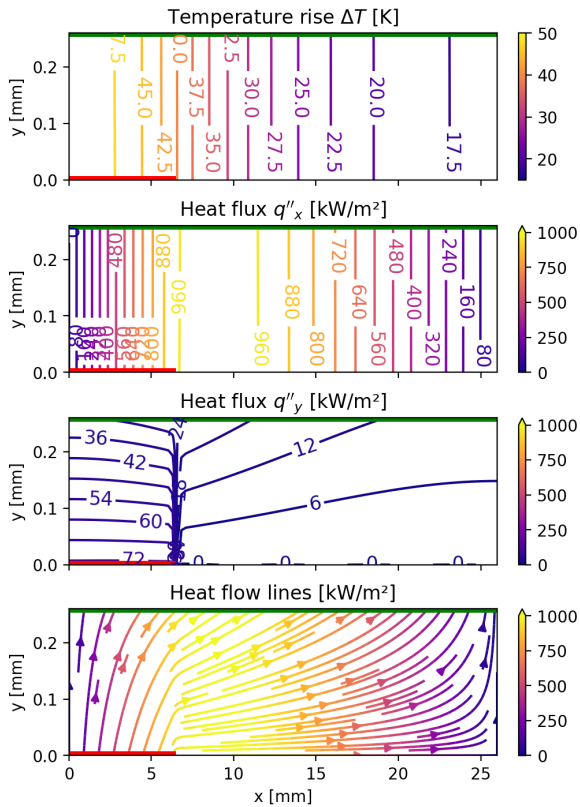


Fig. 13: Temperature rise and heat flux fields for the computed point

during the development of the analytical model. In particular, a copper monoblock cannot faithfully represent a four-layer PCB. The important thing here is the proposed approach. This approach needs to be adapted for multi-layer objects but can already be applied to cooling at the electric potential.

4.5 Comparison with 2D and 3D FEM and perspectives

Firstly, the model is compared to a 2D FEM equivalent model. Results show an almost perfect match on the several tested configurations. The relative RMS error of the order of 10 ppm, which is negligible. This error is due to Gibbs Phenomenon.

Secondly, 3D FEM is introduced. The proposed model suffers from several approximations, one of which is the choice of a 2D formulation. By considering it null, the flux in the third dimension, an essential part of the flux, is neglected. Consequently, the thermal resistance is overestimated. The present formulation was preferred because it allows a calculation with simple Fourier series, where a cylindrical model would require the resolution of Fourier-Bessel series and a 3D rectangular model

would require the resolution of 2D Fourier series.

A finite element simulation is performed to try to quantify the error, in a 3D square configuration, with the parameters determined previously. The component is considered square and placed in the center of a square conductive block. The temperature increase is then 21 K against 42 K previously. This error of a factor 2 is not negligible and requires deeper investigation. Two ideas are considered: quantify the error for the dimensionless values of the Table 2 and determine trends, or solve the 3D problem using the 2D Fourier series.

Thirdly, most of the devices require the consideration of at least three layers of different materials, but the resolution presented is limited to a homogeneous material, so a multilayer study will have to be conducted. This study could be based on an analytical resolution or finite element simulations using a relevant nondimensionalization.

5 Conclusion

The application studied aims at creating an elementary converter (HBC) capable of transmitting high currents on a PCB substrate to reduce the cost. Therefore, it requires thermal cooling because it is a limiting phenomenon.

This work highlights and interprets the phenomena involved in the cooling of power electronics components. The critical parameters and their influence are highlighted using non dimensional groups which are useful tools for an electronic engineer designing a cooling system. For this purpose, two sizing methods are proposed, based on a direct numerical calculation.

However, most devices are constituted of several layers of materials than the model developed in this paper cannot consider. Moreover, a transient study introducing the notion of thermal capacity can be interesting for some applications with significant power variations. Lastly, 2D modeling overestimates the temperature rise of the targeted 3D applications, a study of this error is envisaged to better approximate real situations.

6 Acknowledgments

This paper has been achieved within IBIS project, which is funded by ADEME (*Agence de*

l'environnement et de la maîtrise de l'énergie) through "Le Programme d'investissements d'avenir (PIA)".

References

- [1] C. Chan, "Overview of Electric, Hybrid, and Fuel Cell Vehicles," in *Encyclopedia of Automotive Engineering*, John Wiley & Sons, Ltd, 2014, pp. 1–14. DOI: 10 . 1002 / 9781118354179.auto061.
- [2] M. Ehsani, Y. Gao, S. Longo, and K. M. Ebrahimi, *Modern Electric, Hybrid Electric, and Fuel Cell Vehicles*, Third. Boca Raton: CRC Press, Mar. 2018. DOI: 10 . 1201 / 9780429504884.
- [3] M. Ehsani, K. V. Singh, H. O. Bansal, and R. T. Mehrjardi, "State of the Art and Trends in Electric and Hybrid Electric Vehicles," *Proceedings of the IEEE*, vol. 109, no. 6, pp. 967–984, Jun. 2021. DOI: 10.1109/JPROC.2021.3072788.
- [4] C. Mayet, D. Labrousse, R. Bkekri, F. Roy, and G. Pongnot, "Energetic Macroscopic Representation and Inversion-Based Control of a Multi-Level Inverter with Integrated Battery for Electric Vehicles," in *2021 IEEE Vehicle Power and Propulsion Conference (VPPC)*, Gijon, Spain: IEEE, Oct. 2021, pp. 1–6. DOI: 10.1109/VPPC53923.2021.9699228.
- [5] C. Mayet, D. Labrousse, A. Dittrick, B. Revol, R. Bkekri, and F. Roy, "Simulation and Control of a New Integrated Battery System for Automotive Applications," in *PCIM Europe Digital Days 2021; International Exhibition and Conference for Power Electronics, Intelligent Motion, Renewable Energy and Energy Management*, May 2021, pp. 1–6.
- [6] H. S. Carslaw and J. C. Jaeger, *Conduction of Heat in Solids*, Second Ed. Oxford: Clarendon press, 1959.
- [7] S. Song and K. P. Moran, "Constriction/spreading resistance model for electronics packaging," in *ASME/JSME Thermal Engineering Conference*, 1995, p. 8.
- [8] F. N. Masana, "A closed form solution of junction to substrate thermal resistance in semiconductor chips," *IEEE Transactions on Components, Packaging, and Manufacturing Technology: Part A*, vol. 19, no. 4, pp. 539–545, Dec. 1996. DOI: 10.1109/95.554935.
- [9] Y. Koito, S. Okamoto, and T. Tomimura, "Two-Dimensional Numerical Investigation on Applicability of 45° Heat Spreading Angle," *Journal of Electronics Cooling and Thermal Control*, vol. 4, no. 1, pp. 1–11, Mar. 2014. DOI: 10.4236/jectc.2014.41001.